8-9-2021

Modulation of the effects of class Ib antiarrhythmics on cardiac NaV1.5-encoded channels by accessory NaVβ subunits

Wandi Zhu

Wei Wang

Paweorn Angsutararux

Rebecca L. Mellor

Lori L. Isom

See next page for additional authors

Authors

Wandi Zhu, Wei Wang, Paweorn Angsutararux, Rebecca L. Mellor, Lori L. Isom, Jeanne M. Nerbonne, and Jonathan R. Silva

JCI insight

Modulation of the effects of class Ib antiarrhythmics on cardiac $Na_V1.5$-encoded channels by accessory $Na_V\beta$ subunits

Wandi Zhu, … , Jeanne M. Nerbonne, Jonathan R. Silva

JCI Insight. 2021;6(15):e143092. https://doi.org/10.1172/jci.insight.143092.

Research Article | Cardiology | Therapeutics

Graphical abstract

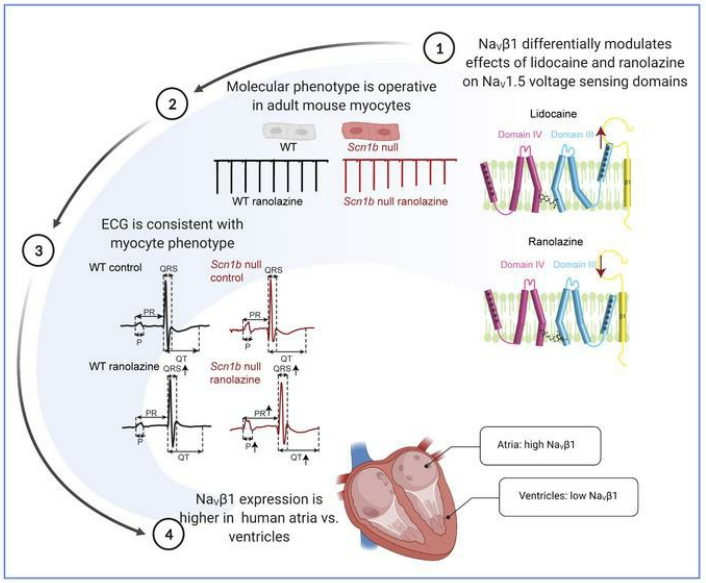

Find the latest version:

https://jci.me/143092/pdf

JCI insight

RESEARCH ARTICLE

Modulation of the effects of class Ib antiarrhythmics on cardiac $Na_V1.5$-encoded channels by accessory $Na_V\beta$ subunits

Wandi Zhu,[1,2] Wei Wang,[3] Paweorn Angsutararux,[1] Rebecca L. Mellor,[3] Lori L. Isom,[4] Jeanne M. Nerbonne,[3,5] and Jonathan R. Silva[1]

[1]Department of Biomedical Engineering, McKelvey School of Engineering, Washington University in St. Louis, St. Louis, Missouri, USA. [2]Department of Medicine, Brigham and Women's Hospital, Boston, Massachusetts, USA. [3]Department of Internal Medicine, Washington University School of Medicine in St. Louis, St. Louis, Missouri, USA. [4]Department of Pharmacology, University of Michigan Medical School, Ann Arbor, Michigan, USA. [5]Department of Developmental Biology, Washington University School of Medicine in St. Louis, St. Louis, Missouri, USA.

Native myocardial voltage-gated sodium (Na_V) channels function in macromolecular complexes comprising a pore-forming (α) subunit and multiple accessory proteins. Here, we investigated the impact of accessory $Na_V\beta1$ and $Na_V\beta3$ subunits on the functional effects of 2 well-known class Ib antiarrhythmics, lidocaine and ranolazine, on the predominant Na_V channel α subunit, $Na_V1.5$, expressed in the mammalian heart. We showed that both drugs stabilized the activated conformation of the voltage sensor of domain-III (DIII-VSD) in $Na_V1.5$. In the presence of $Na_V\beta1$, the effect of lidocaine on the DIII-VSD was enhanced, whereas the effect of ranolazine was abolished. Mutating the main class Ib drug-binding site, F1760, affected but did not abolish the modulation of drug block by $Na_V\beta1/\beta3$. Recordings from adult mouse ventricular myocytes demonstrated that loss of *Scn1b* ($Na_V\beta1$) differentially affected the potencies of lidocaine and ranolazine. In vivo experiments revealed distinct ECG responses to i.p. injection of ranolazine or lidocaine in WT and *Scn1b*-null animals, suggesting that $Na_V\beta1$ modulated drug responses at the whole-heart level. In the human heart, we found that *SCN1B* transcript expression was 3 times higher in the atria than ventricles, differences that could, in combination with inherited or acquired cardiovascular disease, dramatically affect patient response to class Ib antiarrhythmic therapies.

Introduction

Inward Na^+ currents (I_{Na}) carried by voltage-gated (Na_V) channels underlie the initiation and propagation of action potentials in the atria and ventricles (1). Functional Na_V channels reflect the assembly of the 4 homologous domains (DI–DIV) in the pore-forming (α) subunit that are connected by intracellular linkers. Each domain contains 6 transmembrane segments (S1–S6). S1–S4 form the voltage-sensing domains (VSDs). The VSDs undergo conformational changes upon membrane depolarization, which open the pore (S5–S6), enabling inward Na^+ flux (2). Native myocardial Na_V channels function in macromolecular protein complexes, containing many regulatory and anchoring proteins that differentially affect channel function and localization based on the cell type (3). $Na_V\beta$ subunits are essential components of these macromolecular complexes. There are 5 different types of $Na_V\beta$ subunits, $Na_V\beta1$, $Na_V\beta1B$, $Na_V\beta2$, $Na_V\beta3$, and $Na_V\beta4$. $Na_V\beta1$, $Na_V\beta1B$, and $Na_V\beta3$ interact with the Na_V α subunits noncovalently; $Na_V\beta2$ and $Na_V\beta4$ are linked covalently through the formation of disulfide bonds (4). $Na_V\beta1$, $Na_V\beta2$, $Na_V\beta3$, and $Na_V\beta4$ are transmembrane proteins, whereas $Na_V\beta1B$ is secreted (5). Consistent with a crucial role for $Na_V\beta$ subunits in maintaining normal heart function, variants in the genes encoding $Na_V\beta$ subunits have been linked to cardiac rhythm disorders, including Brugada syndrome, long QT syndrome, and sick sinus syndrome (4). However, recent evidence suggests that SCN1B may not be a monogenic cause of Brugada or sudden arrhythmic death syndrome (6, 7). $Na_V\beta1$ and $Na_V\beta1B$, splice variants of *SCN1B*, are the dominant $Na_V\beta$ subunits in the mammalian heart (8).

Although $Na_V\beta$ subunits were first cloned from a rat brain in the 1990s (9), the molecular interactions between $Na_V\alpha$-$Na_V\beta$ subunits have remained elusive until recently. The cryo-electron microscopy structures of the $Na_V1.4$-$Na_V\beta1$ and the $Na_V1.7$-$Na_V\beta1$-$Na_V\beta2$ complexes suggest that $Na_V\beta1$ coassembles with Na_V α

Conflict of interest: The authors have declared that no conflict of interest exists.

Submitted: August 7, 2020
Accepted: June 17, 2021
Published: August 9, 2021

Reference information: *JCI Insight*. 2021;6(15):e143092. https://doi.org/10.1172/jci.insight.143092.

subunits near the domain-III VSD (DIII-VSD) (10–12). However, the recent structure of $Na_V1.5$ revealed that $Na_V\beta1$ interacts with the predominant cardiac Na_V α subunit at a distinct site or sites that are characterized by weaker binding and an unresolvable $Na_V1.5$-$Na_V\beta1$ complex (13). This difference in comparison with channels encoded by other Na_V α subunits is partially due to the unique N-linked glycosylation of $Na_V1.5$ that hinders its interaction with the Ig domain of $Na_V\beta1$ (13). Intriguingly, $Na_V\beta1$ and $Na_V\beta3$ are highly homologous except in the Ig domains. Previously, optical tracking of the $Na_V1.5$ VSDs using voltage-clamp fluorometry (VCF) revealed that the $Na_V\beta3$ subunit modulates both the DIII and the DIV-VSDs, whereas $Na_V\beta1$ only modulates the DIV-VSD conformational dynamics (14, 15). Fluorescence quenching experiments showed that the DIII-VSD is in close proximity to $Na_V\beta3$ but not $Na_V\beta1$ (14). These results suggest that $Na_V\beta1$ and $Na_V\beta3$ regulate the $Na_V1.5$ DIII-VSD differently.

The conformational changes in the VSDs are not only important for regulating channel gating; they are also essential for modulating channel interactions with drugs, including those that bind to the pore domain, such as local anesthetics (16). Previously, VCF and gating current recordings showed that when lidocaine blocks $Na_V1.4$ channels, it stabilizes the DIII-VSD in its activated conformation (17). Moreover, we recently demonstrated that alteration of DIII-VSD conformational changes caused by long QT syndrome 3 variants leads to channels with different mexiletine sensitivities (18, 19).

Class I antiarrhythmics modulate cardiomyocyte excitability via Na_V channel targeting. Class Ib molecules, such as lidocaine, ranolazine, and mexiletine, specifically modulate the late component of I_{Na}, resulting in shortening of the action potential duration in ventricular cardiomyocytes (20). Lidocaine has long been used to manage ventricular arrhythmias in hospital settings (21). Ranolazine has been shown to be effective in controlling various cases of atrial fibrillation (AF) (22–24), particularly paroxysmal AF (25, 26). Recently, the RAID trial demonstrated that ranolazine also marginally lowered the risk of recurrent ventricular tachycardia and ventricular fibrillation in high-risk patients with implanted cardioverter-defibrillators (27). Although both drugs are commonly prescribed for several arrhythmias, their efficacies are highly variable. Thus, it remains an important task to understand the determinants of channel-drug interactions that contribute to this variability.

In the experiments presented here, we aimed to understand the molecular mechanisms whereby noncovalently bound $Na_V\beta$ subunits modulate the interaction of class Ib antiarrhythmics with myocardial $Na_V1.5$ channels. We further investigated the physiological significance of this modulation by assessing ranolazine and lidocaine drug blockade of native Na_V currents in mouse ventricular myocytes, probing the mRNA expression levels of $Na_V\beta$ subunits in human hearts and detailing the in vivo electrophysiological phenotypes evident in the cardiac-specific *Scn1b*-null mouse (28). Our results showed a critical role for β subunits in differentially modulating the efficacy of lidocaine and ranolazine, implying that patient-to-patient differences in β subunit expression are likely to have a significant impact on therapeutic outcomes.

Results

Both lidocaine and ranolazine alter $Na_V1.5$ DIII-VSD dynamics. Previous studies demonstrated that lidocaine shifts the activation of the DIII-VSD in rat $Na_V1.4$ channels encoded by *Scn4a* and prominent in skeletal muscle in the hyperpolarizing direction (16, 29, 30). Recent findings showed that a class Ib antiarrhythmic, mexiletine, which is similar in structure to lidocaine, also affects the DIII-VSD conformation in $Na_V1.5$ channels (18, 19). The DIII-VSD effect also determines the tonic and use-dependent properties of class Ib drugs (18, 19). Taken together, these observations suggest that factors that alter drug effects on the DIII-VSD would be expected to have an impact on therapeutic efficacy.

To explore this hypothesis, we first used VCF to assess the effects of 2 class Ib antiarrhythmics, lidocaine and ranolazine (Figure 1A), on the DIII-VSD in heterologously expressed human $Na_V1.5$ channels, which are encoded by *SCN5A*, the predominant Na_V α subunit expressed in the mammalian heart (Figure 1, B and C). When we expressed the $Na_V1.5$ α subunit alone in *Xenopus* oocytes, we observed a hyperpolarizing shift ($\Delta V_{1/2}$ = –24.8 ± 9.4 mV, P = 0.03) in the DIII fluorescence-voltage (F-V) curve on exposure to 10 mM lidocaine, and a similar shift ($\Delta V_{1/2}$ = –30.7 ± 7.5 mV, P = 0.05) on application of 4 mM ranolazine, suggesting that both lidocaine and ranolazine stabilize the DIII-VSD in its activated conformation (Figure 1, B–D). The observation of similar effects on the DIII-VSD caused by both drugs is not surprising because they share similar molecular structures (Figure 1A), shown previously to interact with residue F1760 in DIV-S6 (20, 31). In addition, however, the effects of lidocaine and ranolazine are not identical. Lidocaine, for example, induced a hyperpolarizing shift in the DIV F-V curve, an effect not observed with ranolazine

(Figure 1, B–D), suggesting that despite sharing common binding motifs on the $Na_V1.5$ α subunit, the distinct chemical structures of lidocaine and ranolazine (Figure 1A) uniquely regulate DIV-VSD dynamics.

$Na_V\beta1$ and $Na_V\beta3$ differentially modulate lidocaine/ranolazine effects on the DIII-VSD. We have previously shown that both $Na_V\beta1$ and $Na_V\beta3$ alter DIII-VSD dynamics during $Na_V1.5$ channel gating (14). Thus, we hypothesized that these $Na_V\beta$ subunits will also alter the effects of class Ib antiarrhythmics on the DIII-VSD. To test this hypothesis, we coexpressed $Na_V1.5$ with the $Na_V\beta1$ or $Na_V\beta3$ subunit and measured DIII-VSD and DIV-VSD conformational changes before and after lidocaine or ranolazine application.

When we coexpressed $Na_V1.5$ with $Na_V\beta1$, we observed distinct DIII-VSD responses to lidocaine and ranolazine. Lidocaine induced a greater hyperpolarizing shift ($\Delta V_{1/2}$ = –57.6 ± 10.2 mV, P = 0.01) in DIII-FV (Figure 2A) when $Na_V\beta1$ was present compared with the $Na_V1.5$ α subunit expressed alone. Exposure to ranolazine, in marked contrast, did not result in a significant DIII-FV shift ($\Delta V_{1/2}$ = –12.8 ± 16.8 mV, P = 0.53) (Figure 2C), suggesting that the DIII-VSD was free to move in $Na_V1.5$ channels in the presence of $Na_V\beta1$ to recover to the resting state. Although the presence of $Na_V\beta1$ increased the lidocaine effect on the DIII-VSD, $Na_V\beta1$ coexpression eliminated the ranolazine effect.

Strikingly, coexpression with the $Na_V\beta3$ subunit resulted in opposite effects on lidocaine and ranolazine interaction with the DIII-VSD. Upon lidocaine block, the DIII F-V curve was minimally shifted to more hyperpolarized potentials ($\Delta V_{1/2}$ = –25.3 ± 10.9 mV, P = 0.13) (Figure 2B), while the ranolazine effect on the DIII-VSD was potentiated, resulting in a larger hyperpolarizing shift in the DIII F-V ($\Delta V_{1/2}$ = 58.0 ± 4.7 mV, P < 0.001) (Figure 2D).

Additionally, coexpression of $Na_V\beta1$ or $Na_V\beta3$ with $Na_V1.5$ both eliminated the hyperpolarizing shift in the DIV F-V curve that was observed with the $Na_V1.5$ α subunit expressed alone (Figure 2, A and B), suggesting that the $Na_V\beta1$ and $Na_V\beta3$ subunits similarly altered lidocaine's effect on the DIV-VSD.

These results demonstrated that $Na_V\beta$ subunits differentially regulated lidocaine and ranolazine interactions with the DIII-VSD in heterologously expressed $Na_V1.5$ channels. Specifically, $Na_V\beta1$ enhanced the effect of lidocaine but decreased the effect of ranolazine on the DIII-VSD activation, whereas $Na_V\beta3$ coexpression had the opposite effects on both drugs. The altered drug interactions with the DIII-VSD resulted in an enhanced block by lidocaine and reduced block by ranolazine when the $Na_V1.5$ α subunit was coexpressed with $Na_V\beta1$ compared with $Na_V\beta3$ (Figure 3C).

To determine whether the differential modulation of lidocaine and ranolazine block by $Na_V\beta1$ and $Na_V\beta3$ is dependent on the main local anesthetic binding site F1760 (20, 31) (Figure 3A), we assessed drug blockade of the F1760A-mutant $Na_V1.5$ channel in the presence of $Na_V\beta1$ or $Na_V\beta3$. As expected, the F1760A-mutant channels exhibited much reduced block by lidocaine and ranolazine compared with the WT channels (Figure 3, C and D). However, application of 10 mM lidocaine or 4 mM ranolazine still caused significant tonic block (TB) and use-dependent block (UDB) of the F1760A channels (Figure 3, D and E). TB reflects resting-state drug block, while UDB requires prior channel opening (32). In contrast to the WT channels, the hyperpolarizing shift in the DIII F-V upon lidocaine or ranolazine block was not observed with the F1760A-mutant channels (Figure 3B). The F1760A mutation also eliminated $Na_V\beta1$ and $Na_V\beta3$ modulation of TB by lidocaine and ranolazine as well as UDB by lidocaine (Figure 3, D and E). However, despite the absence of a major drug-binding site, coexpression of $Na_V\beta3$ still caused stronger UDB by ranolazine compared with $Na_V\beta1$ (Figure 3E). These results suggest that the effects of $Na_V\beta1/\beta3$ on lidocaine and ranolazine block are affected by the F1760 anesthetic binding site but are not completely dependent on it.

Loss of Scn1b expression in mouse cardiomyocytes does not affect Na_V channel gating. To further investigate how noncovalent $Na_V\beta1/\beta1B$ subunits affect the cardiomyocyte response to class Ib antiarrhythmics, we utilized the cardiac-specific *Scn1b*-null mouse model (*$Scn1b^{fl/fl}$/Myh6-cre*) described previously (28). First, we compared I_{Na} in left ventricular (LV) myocytes acutely dissociated from adult *Scn1b* cardiac-specific null and WT mice. Peak I_{Na} density was increased by 28% in *Scn1b*-null compared with WT LV myocytes (*Scn1b*-null: 81.3 ± 3.6 pA/pF, WT: 63.9 ± 5.2 pA/pF, P = 0.017). An increase in I_{Na} density in cardiac-specific *Scn1b*-null isolated from juvenile mice was previously reported (28). Consistent with the increase in current density, we also observed increased *Scn5a* transcript expression in the ventricles (and atria) of the *Scn1b*-null compared with WT mice (Supplemental Figure 1; Supplemental material available online with this article; https://doi.org/10.1172/jci.insight.143092DS1). Other than increasing peak current density, *Scn1b* deletion did not measurably alter other Na_V channel gating properties in ventricular cardiomyocytes (Figure 4A), including the voltage dependences of channel activation (Figure 4B), steady-state inactivation (Figure 4B), and/or the

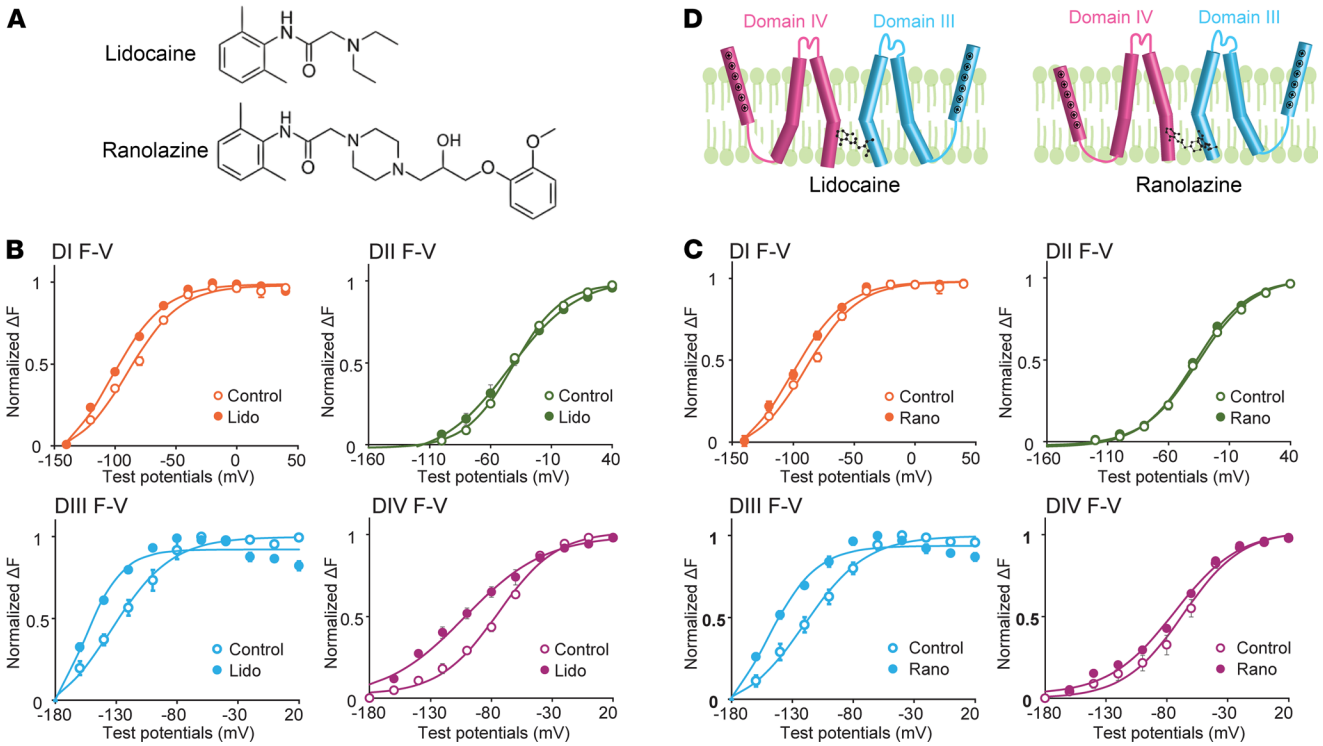

Figure 1. Class Ib antiarrhythmics lidocaine and ranolazine alter $Na_V1.5$ VSD conformations. (**A**) Chemical structures of lidocaine and ranolazine. (**B**) Voltage dependence of the steady-state fluorescence (F-V curves) from the 4 domains (DI-V215C, DII-S805C, DIII-M1296C, DIV-S1618C) of $Na_V1.5$ before and after 10 mM lidocaine. Lidocaine was used at 10 mM to produce a robust tonic block (TB). In the presence of lidocaine, fluorescence was measured when TB reached more than 70%. Lidocaine induced a hyperpolarizing shift in both the DIII and DIV F-V curves. (**C**) F-V curves from the 4 domains of $Na_V1.5$ before and after 4 mM ranolazine. Similar to the lidocaine experiment (**B**), in the presence of ranolazine, the fluorescence was measured when TB reached more than 70%. Ranolazine caused a hyperpolarizing shift in the DIII but not in the DIV F-V curve. (**D**) Schematic showing effects of lidocaine and ranolazine on the DIII- and DIV-VSDs; note that each VSD is represented by a single S4 segment for clarity. Lidocaine caused both the DIII and the DIV VSDs to stabilize in the activated conformation, whereas ranolazine only stabilized the DIII-VSD in the activated position. Each data set represents mean ± SEM values from 4–6 cells.

kinetics of channel recovery from inactivation (Figure 4C). Notably, deleting *Scn1b* did not measurably alter the expression of other $Na_V\beta$ subunits (Supplemental Figure 1). These results, although contrary to previously reported effects of $Na_V\beta1$ on I_{Na} in heterologous expression systems, are consistent with results obtained in studies on global and cardiac-specific *Scn1b*-null mice (28, 33).

Increased block of I_{Na} by ranolazine but reduced block by lidocaine in adult Scn1b-null mouse ventricular myocytes. Even though Na_V channel gating was not measurably affected in cardiac-specific *Scn1b*-null myocytes, we went on to determine whether the loss of *Scn1b* affects the responses of native Na_V channels to class Ib antiarrhythmics. We examined the effects of lidocaine and ranolazine on TB and UDB of I_{Na} in LV myocytes isolated from WT and cardiac-specific *Scn1b*-null mice.

The TB produced by 100 μM lidocaine was similar in WT and *Scn1b*-null LV myocytes (Figure 5A). In marked contrast, the block of late I_{Na} by lidocaine was significantly reduced in *Scn1b*-null LV myocytes (Figure 5B). There was also an approximately 3-fold reduction in lidocaine UDB in *Scn1b*-null compared with WT LV myocytes (WT: EC_{50UDB} = 9.3 μM, *Scn1b*-null EC_{50UDB} = 24.8 μM) (Figure 5E). Conversely, ranolazine increased TB, late I_{Na} block, and UDB in *Scn1b*-null compared with WT adult mouse LV myocytes (Figure 5, C, D, and F) (WT: EC_{50UDB} = 53.3 μM, *Scn1b*-null EC_{50UDB} = 36.0 μM). The differences in UDB by lidocaine between WT and *Scn1b*-null myocytes depended on the frequency and duration of the depolarizing pulses (Figure 5G). In response to 10 μM lidocaine, I_{Na} from *Scn1b*-null showed decreased UDB compared with WT myocytes at 10 Hz (25 ms duration) and 2 Hz (400 ms duration) but not 5 Hz (25 ms duration) (Figure 5G). In contrast, in response to 10 μM ranolazine, I_{Na} in WT myocytes showed increased UDB compared with Scn1b-null myocytes at all 3 frequencies (Figure 5H). Both lidocaine and ranolazine are known to cause a hyperpolarizing shift in the voltage dependence of steady-state inactivation of cardiac I_{Na} (24, 34), indicating that drug binding promotes channel inactivation at more hyperpolarized membrane potentials. Therefore, we also compared the voltage dependence of I_{Na} inactivation in WT and *Scn1b*-null LV

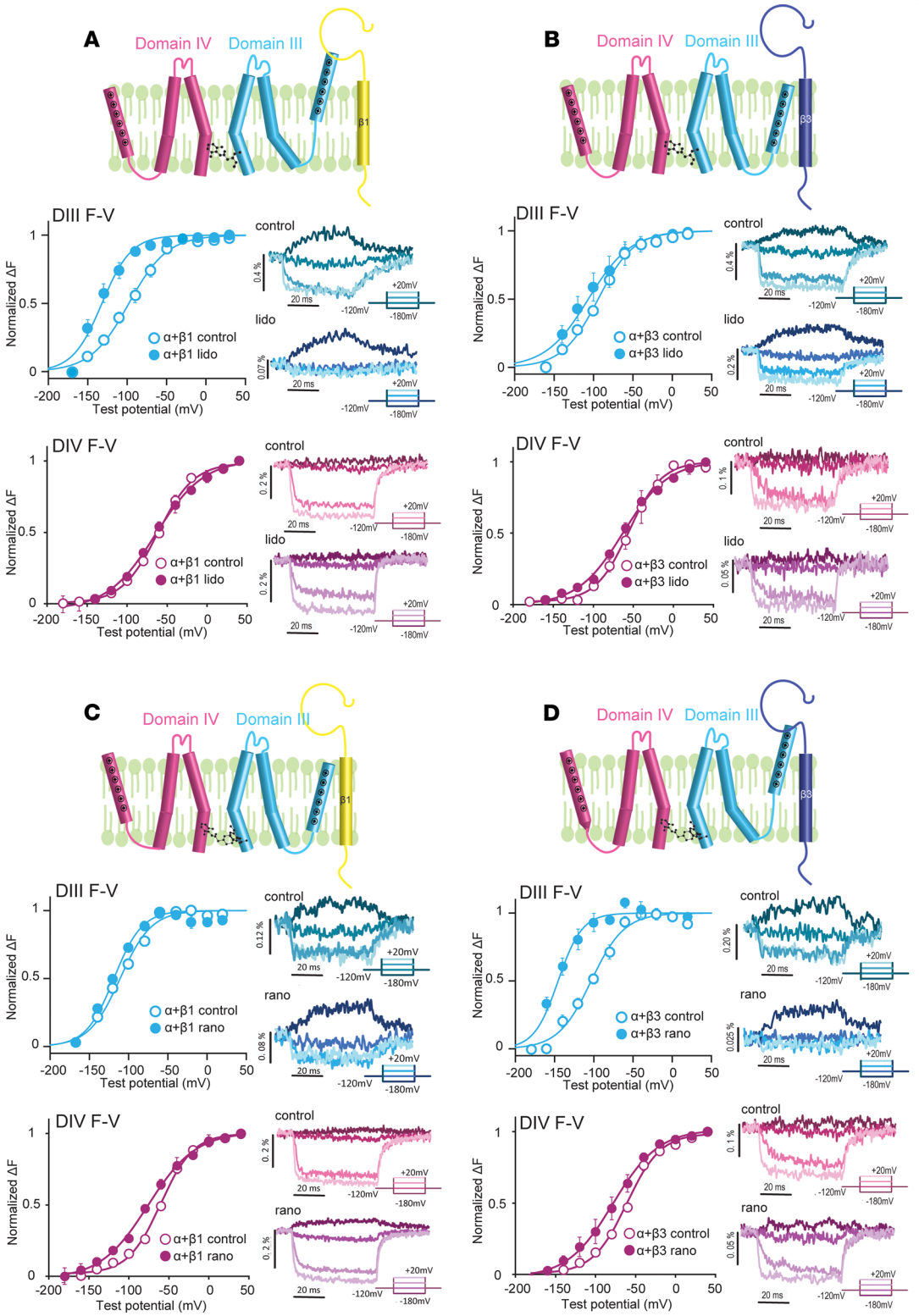

Figure 2. Coexpression with $Na_v\beta1$ or $Na_v\beta3$ differentially modulates the effect of lidocaine and ranolazine on the DIII-VSD. (**A**) In the presence of $Na_v\beta1$, the hyperpolarizing shift in the DIII F-V curve produced by lidocaine was enhanced compared with the $Na_v1.5$ α subunit expressed alone. In marked contrast, the DIV F-V curve was not affected by lidocaine with $Na_v\beta1$ present. (**B**) In contrast with $Na_v\beta1$ (**A**), the hyperpolarized shift in the DIII F-V curve induced by lidocaine was eliminated when $Na_v\beta3$ was coexpressed. Similar to $Na_v\beta1$, however, the DIV F-V curve was minimally affected by lidocaine. (**C**) In the presence of $Na_v\beta1$, the effect of ranolazine on the DIII F-V curve was eliminated, whereas the DIV F-V was slightly hyperpolarized. (**D**) In contrast with $Na_v\beta1$ (**C**), the hyperpolarized shift in the DIII F-V curve caused by ranolazine was enhanced when $Na_v\beta3$ was coexpressed. In the presence of $Na_v\beta3$, ranolazine also caused a small hyperpolarizing shift in the DIV F-V curve. Each data set represents mean ± SEM values from 4–6 cells.

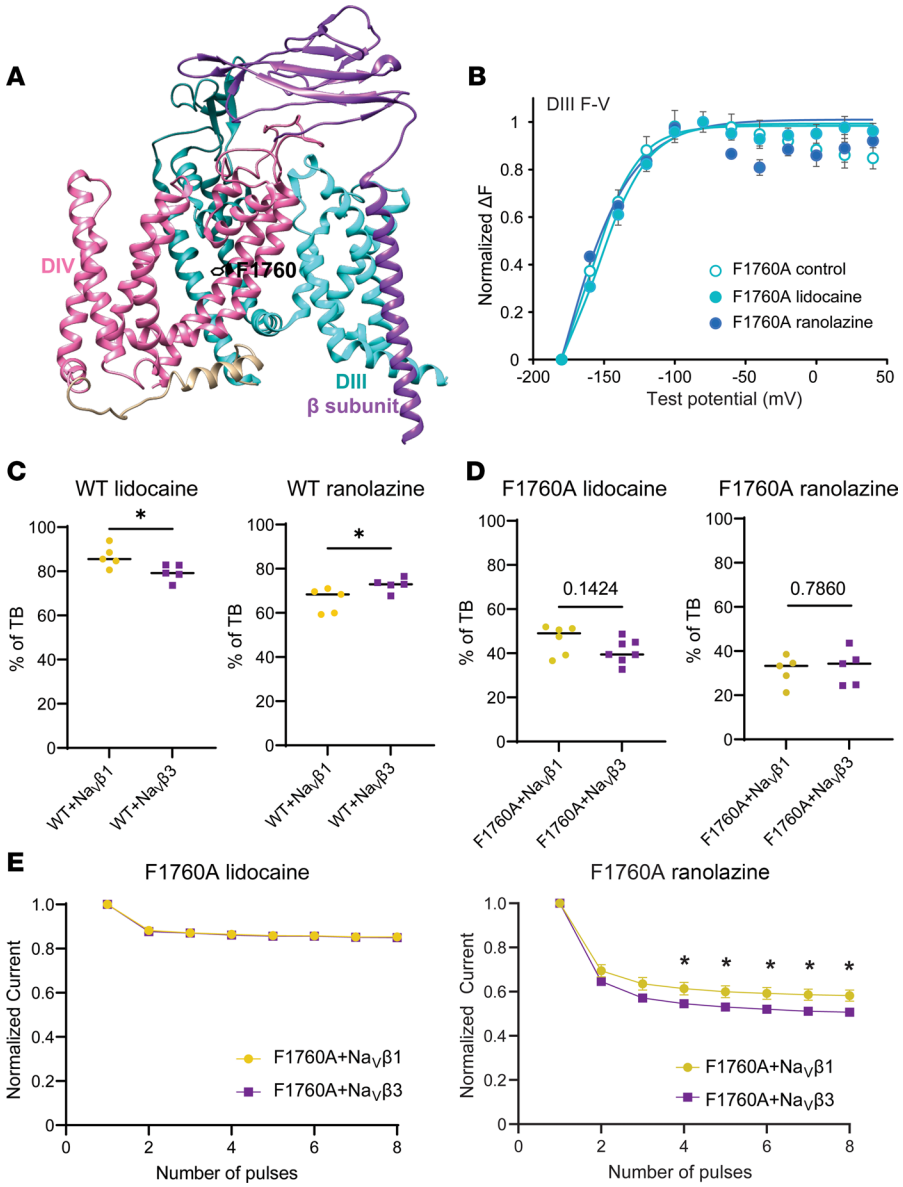

Figure 3. Altering the key local anesthetics' binding site F1760 did not completely abolish $Na_V\beta1/\beta3$ modulations of ranolazine block. (**A**) Cryo-electron microscopy structure of human $Na_V1.4$(11) (Protein Data Bank 6AGF) showing the relative locations of the F1760 residue, DIII, DIV, and $Na_V\beta1$. (**B**) Mutating the main local anesthetic binding residue F1760 to alanine (**A**) greatly reduced the hyperpolarizing shift in the DIII-VSD upon 10 mM lidocaine, as well as 4 mM ranolazine, observed in the WT channel (Figures 1 and 2). (**C**) Percentage of TB induced by 10 mM lidocaine and 4 mM ranolazine in the WT channel. The presence of $Na_V\beta3$ reduced lidocaine TB but enhanced ranolazine TB compared with the α-$Na_V\beta1$ complex. (**D**) Percentage of TB induced by 10 mM lidocaine and 4 mM ranolazine in the F1760A channel. In contrast to WT, $Na_V\beta1$ and $Na_V\beta3$ no longer exerted a significant effect on lidocaine and ranolazine TB. (**E**) UDB by lidocaine and ranolazine in F1760A channel coexpressed with $Na_V\beta1$ or $Na_V\beta3$. There was no change in lidocaine UDB comparing coexpression with $Na_V\beta1$ and $Na_V\beta3$. However, the presence of $Na_V\beta1$ caused a reduced ranolazine UDB compared with $Na_V\beta3$, a phenomenon that is similar to $Na_V\beta1$'s effects on the WT channel. Each data set represents mean ± SEM values from 3–6 cells. Unpaired 2-tailed Student's *t* test was used to test significance (**C**–**E**). $^*P < 0.05$.

myocytes before and after lidocaine or ranolazine application. These experiments revealed 100 μM lidocaine induced a hyperpolarizing shift in I_{Na} inactivation in WT LV myocytes and a smaller shift in *Scn1b*-null LV myocytes (Supplemental Figure 2A). Conversely, 100 μM ranolazine induced a comparable leftward shift in the voltage dependence of inactivation of I_{Na} in WT and *Scn1b*-null LV myocytes (Supplemental Figure 2B).

Overall, these cellular studies revealed that in adult mouse LV myocytes, the cardiac deletion of *Scn1b* resulted in reduced lidocaine UDB but increased ranolazine UDB. These results are consistent with our

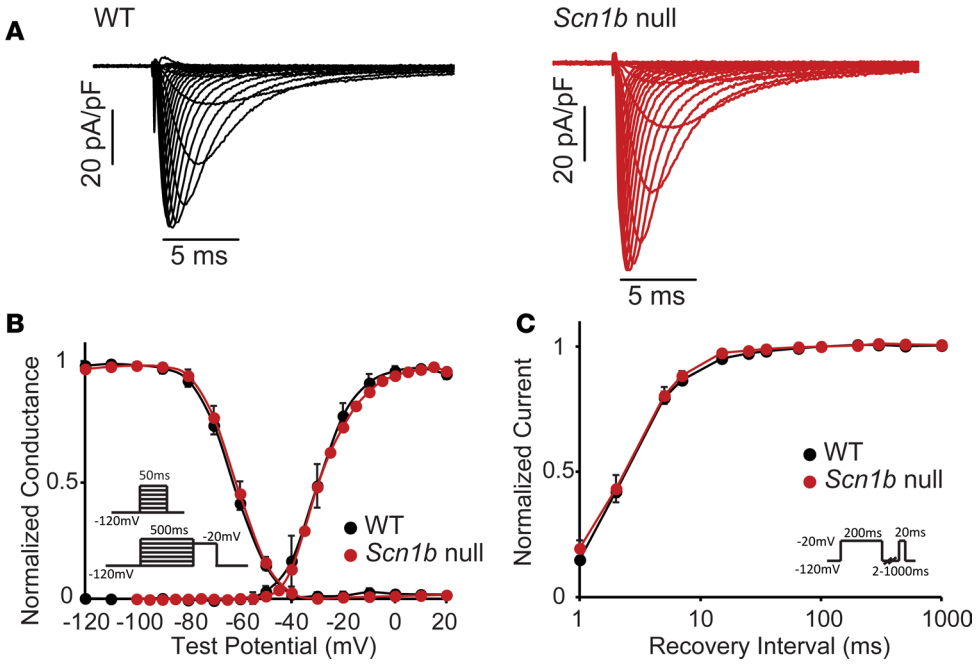

Figure 4. I_{Na} gating is similar in *Scn1b*-null and WT mouse LV myocytes. (**A**) Representative recordings of I_{Na} in WT and *Scn1b*-null mouse LV myocytes revealed similar kinetics of activation and inactivation. However, the average peak current density was slightly (~28%) higher in *Scn1b*-null compared with WT. (**B**) Loss of $Na_V\beta1$ in *Scn1b*-null mouse LV myocytes did not affect the voltage dependences of I_{Na} activation or steady-state inactivation. (**C**) Loss of $Na_V\beta1$ in *Scn1b*-null mouse LV myocytes also did not affect the time course of I_{Na} recovery from inactivation. Each data set represents mean ± SEM values from 6–9 cells.

VCF data (Figures 1 and 2), suggesting that the presence of $Na_V\beta1$ subunits enhanced lidocaine's effects but reduced ranolazine's effects on the $Na_V1.5$ DIII-VSD. The reduced effects on the DIII-VSD are also consistent with the decreased UDB of I_{Na} observed in LV myocytes (Figure 5).

Ranolazine and lidocaine induced distinct ECG phenotypes in WT and Scn1b-null mice. To understand how $Na_V\beta1/\beta1B$ modulate antiarrhythmic responses at the whole-heart level, we measured surface ECGs in anesthetized WT and *Scn1b*-null mice before and after i.p. injection of lidocaine or ranolazine (Figure 6 and Supplemental Table 1). From the raw ECG data, we quantified several parameters that describe overall heart electrical functioning, including RR intervals, providing a measure of heart rates; P wave intervals, representing atrial conduction; PR intervals, characterizing atrial-ventricular conduction; QRS intervals, revealing ventricle conduction; and QT and ST intervals, corresponding to ventricular repolarization.

We found that 20 mg/kg ranolazine caused QRS prolongation in both WT and *Scn1b*-null mice (Figure 6, A and B), but that P wave and PR interval prolongation only occurred in the *Scn1b*-null mice (Figure 6B). The QT interval, but not the ST interval, was also prolonged by ranolazine in *Scn1b*-null mice (Figure 6B and Supplemental Figure 3). These results suggest that *Scn1b* deletion enhanced the inhibitory effect of ranolazine on cardiac conduction. Similar to the effects observed at the single myocyte level (Figures 4 and 5) that the loss of *Scn1b* enhanced TB and UDB of I_{Na} by ranolazine, loss of $Na_V\beta1/\beta1B$ in *Scn1b*-null mice promoted ranolazine block, manifesting as P wave, PR, and QRS interval prolongation.

We observed that 30 mg/kg lidocaine administration increased P wave duration in WT and *Scn1b*-null mice (Figure 6, A and C). In addition, lidocaine induced prolongation of RR, QT, and ST intervals in WT but not *Scn1b*-null mice (Figure 6C and Supplemental Figure 3). In contrast, lidocaine increased PR and QRS intervals in *Scn1b*-null mice (Figure 6C). Lidocaine injection, therefore, resulted in distinct functional effects in the 2 genotypes. We conducted control experiments in which we measured ECGs before and after injection of PBS solution. Comparison of baseline and post-PBS data showed that ECG parameters remained constant (Supplemental Figure 4).

SCN1B is differentially expressed in human atria and ventricles. The observation that loss of *Scn1b* alters the ability of class Ib antiarrhythmics to block Na_V channels in the mouse heart suggests that the differential expression of *SCN1B* might play an important role in regulating antiarrhythmic drug responses in humans.

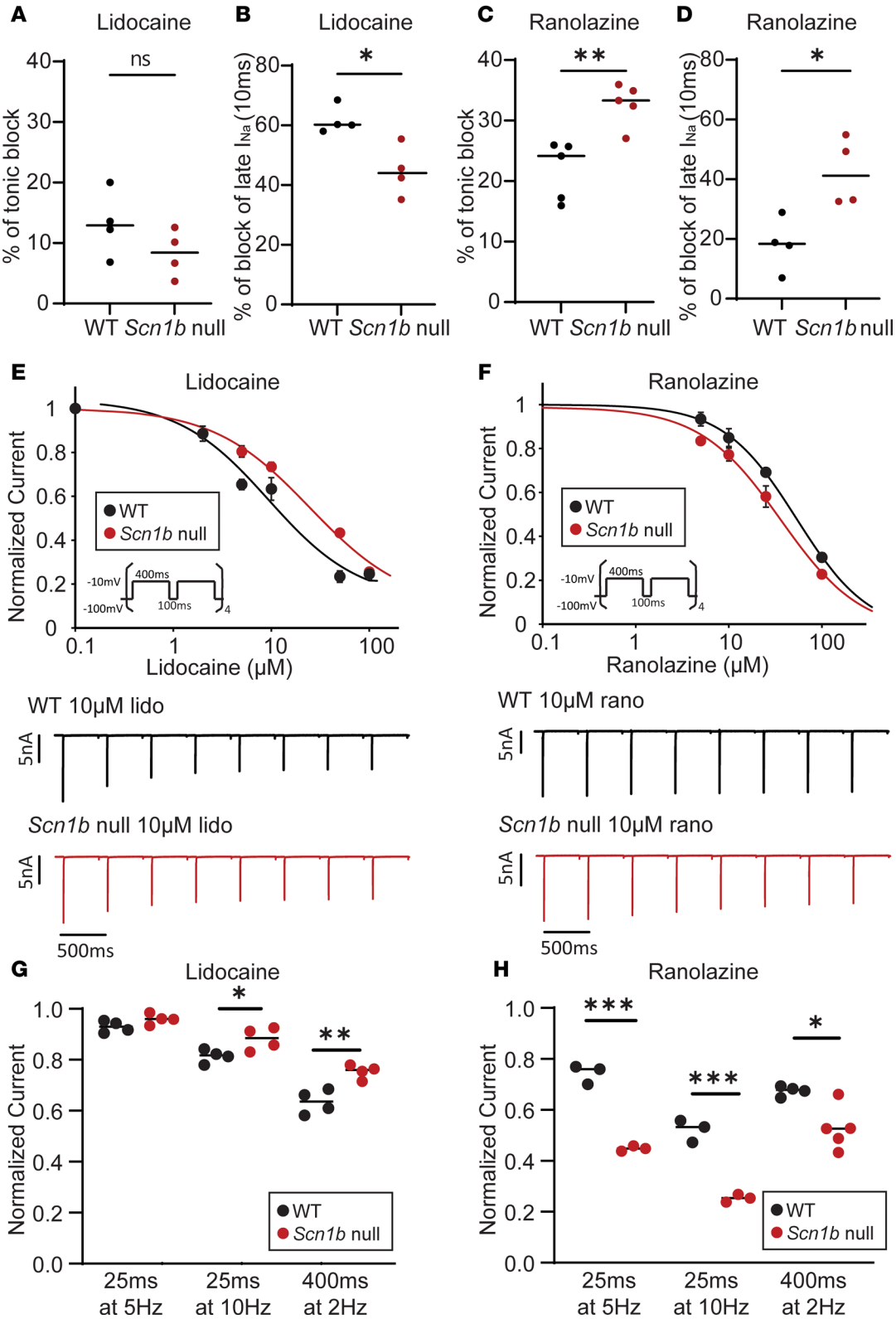

Figure 5. *Scn1b*-null LV myocytes show reduced lidocaine but enhanced ranolazine responses. (**A**) TB of I_{Na} by 100 μM lidocaine was slightly reduced in *Scn1b*-null compared with WT mouse LV myocytes. (**B**) Percentage of late I_{Na} block by 100 μM lidocaine was markedly lower in *Scn1b*-null compared with WT mouse LV myocytes. Late I_{Na} was measured 30 ms after the onset of the depolarizing voltage step. (**C**) TB of I_{Na} by 100 μM ranolazine was greater in *Scn1b*-null compared with WT mouse LV myocytes. (**D**) Percentage of late I_{Na} block by 100 μM ranolazine was greater in *Scn1b*-null compared with WT mouse LV myocytes. (**E**) Dose-response curve (top) and example traces (bottom) for UDB of I_{Na} by lidocaine. UDB was examined by measuring I_{Na} evoked in response to 8 repetitive (400 ms duration) depolarizations presented at 2 Hz, which determines the initial rate of UDB. The EC_{50} for UDB of I_{Na} by lidocaine was lower in WT compared with *Scn1b*-null suggesting that $Na_V\beta1$ enhances the sensitivity to lidocaine. (**F**) Dose-response curve (top) and

example traces (bottom) for UDB of I_{Na} by ranolazine. In contrast to lidocaine, the EC_{50} for UDB by ranolazine was higher in WT compared with *Scn1b*-null, suggesting $Na_V\beta1$ reduces the effects of ranolazine. (**G**) Frequency-dependent UDB block of I_{Na} by 10 μM lidocaine in WT and *Scn1b*-null LV myocytes. UDB was assessed by measuring I_{Na} evoked by repetitive depolarizing pulses at 5 Hz (25 ms, 40 pulses), 10 Hz (25 ms, 40 pulses), and 2 Hz (400 ms, 8 pulses). Normalized currents indicate $I_{Na(last\text{-}pulse)}/I_{Na(first\text{-}pulse)}$. (**H**) Frequency-dependent UDB block of I_{Na} by 10 μM ranolazine in WT and *Scn1b*-null LV myocytes. Each data set represents mean ± SEM of data from 3–5 cells. Unpaired 2-tailed Student's *t* test. $^*P < 0.05$; $^{**}P < 0.01$; $^{***}P < 0.001$.

To begin to explore this hypothesis, we examined mRNA expression levels of the genes *SCN1B*, *SCN2B*, *SCN3B*, and *SCN4B* encoding $Na_V\beta$ subunits in human heart tissue in a recently published RNA-Seq library (35). These analyses revealed that in the human heart, *SCN1B* is the most abundant of the $Na_V\beta$ subunits at the transcript level and that *SCN1B* transcript expression is much higher in atria than in ventricles (Figure 7A). In contrast, the expression levels of the *SCN2B* and *SCN4B* transcripts are higher in the ventricles than in the atria (Figure 7A). To validate the RNA-Seq findings and to determine whether both *SCN1B* splice variants, *SCN1BA* ($Na_V\beta1$) and *SCN1BB* ($Na_V\beta1B$), are differentially expressed in human atria and ventricles, we performed quantitative RT-PCR analyses on the same tissue samples used in the RNA-Seq analyses. These experiments revealed that the relative expression levels of the 2 *SCN1B* splice variants were significantly higher in the atria compared with the ventricles (Figure 7B). Additional analyses revealed that, although expression of *SCN1BA* was approximately 100-fold higher than *SCN1BB*, the expression levels of the 2 (*SCN1BA* and *SCN1BB*) splice variants were similar in human right and left atria and in the LV and right ventricle (RV) (Supplemental Figure 5).

Discussion

Although class Ib antiarrhythmics have considerable therapeutic potential, they are not broadly prescribed because of proarrhythmic risks in some patients and ineffectiveness in others (36, 37). Patient or disease variability in class Ib drug response suggests that there are external factors that modulate drug interactions with the channel (37). In this study, we investigated the role of Na_V channel accessory subunits $Na_V\beta1$ and $Na_V\beta3$ in regulating class Ib antiarrhythmic–mediated effects on $Na_V1.5$ channels. We demonstrated that at a molecular level, $Na_V\beta1$ or $Na_V\beta3$ subunit coexpression differentially altered the effects of lidocaine and ranolazine on the $Na_V1.5$ DIII-VSD. $Na_V\beta1$ enhanced lidocaine but inhibited ranolazine modulation of the DIII-VSD. Conversely, $Na_V\beta3$ eliminated lidocaine modulation but increased the effect of ranolazine on the DIII-VSD. Differential molecular interactions between $Na_V1.5$ DIII-VSD and class Ib antiarrhythmic drugs caused by $Na_V\beta1$ subunit expression in a heterologous system translated to distinct drug blockade of Na_V channels in WT versus *Scn1b* cardiac-specific null mouse cardiomyocytes. We further demonstrated differential effects of lidocaine and ranolazine on the ECG phenotypes of WT and *Scn1b*-null mice.

$Na_V\beta1$ and $Na_V\beta3$ subunits alter $Na_V1.5$ channel pharmacology via the DIII-VSD. The DIII-VSD plays an important role in regulating $Na_V1.5$ channel gating. It is involved in both activation and inactivation of Na_V channels (38, 39). Recent studies showed a correlation between DIII-VSD deactivation and the slow component of recovery from inactivation, which suggests that an activated form of the DIII-VSD stabilizes inactivation (39). Given that class Ib antiarrhythmics promote DIII-VSD activation, they may subsequently promote inactivation to induce greater levels of UDB. We recently demonstrated that DIII-VSD activation determines $Na_V1.5$ channel blockade by mexiletine and affects the sensitivity of LQT3 variants to this drug (18), demonstrating a clear connection between the conformation of the DIII-VSD and class Ib drug potency.

We previously demonstrated that $Na_V\beta3$ directly modulates the DIII-VSD, whereas $Na_V\beta1$ does not (14). Recent channel structures suggest that $Na_V\beta1$ associates with $Na_V1.7$ and $Na_V1.4$ through the DIII-VSD, an interaction that is not conserved in $Na_V1.5$ (10, 12, 13). In light of these structural and functional data, it is plausible that $Na_V\beta3$ interacts with $Na_V1.5$ through similar sites as illustrated in the $Na_V1.4$/$Na_V1.7$-β1 complex, while $Na_V\beta1$ occupies a different site. Two distinct interaction mechanisms will result in the differential modulation of the DIII-VSD by $Na_V\beta1$ and $Na_V\beta3$. Here, we showed that coexpression of the $Na_V\beta1$ or $Na_V\beta3$ subunit differentially modulated the ability of class Ib antiarrhythmics to stabilize the DIII-VSD in the activated conformation, providing further evidence that in contrast to other Na_V channel α subunits, $Na_V\beta1$ and $Na_V\beta3$ have distinct interactions with $Na_V1.5$. The effect of lidocaine on the DIII-VSD has been previously shown (14) to regulate UDB, a critical feature of class Ib drugs, which renders them most potent when myocytes are being excited repeatedly during an arrhythmic event. We observed that ranolazine and lidocaine similarly affected $Na_V1.5$ α subunit–encoded channels expressed in the absence

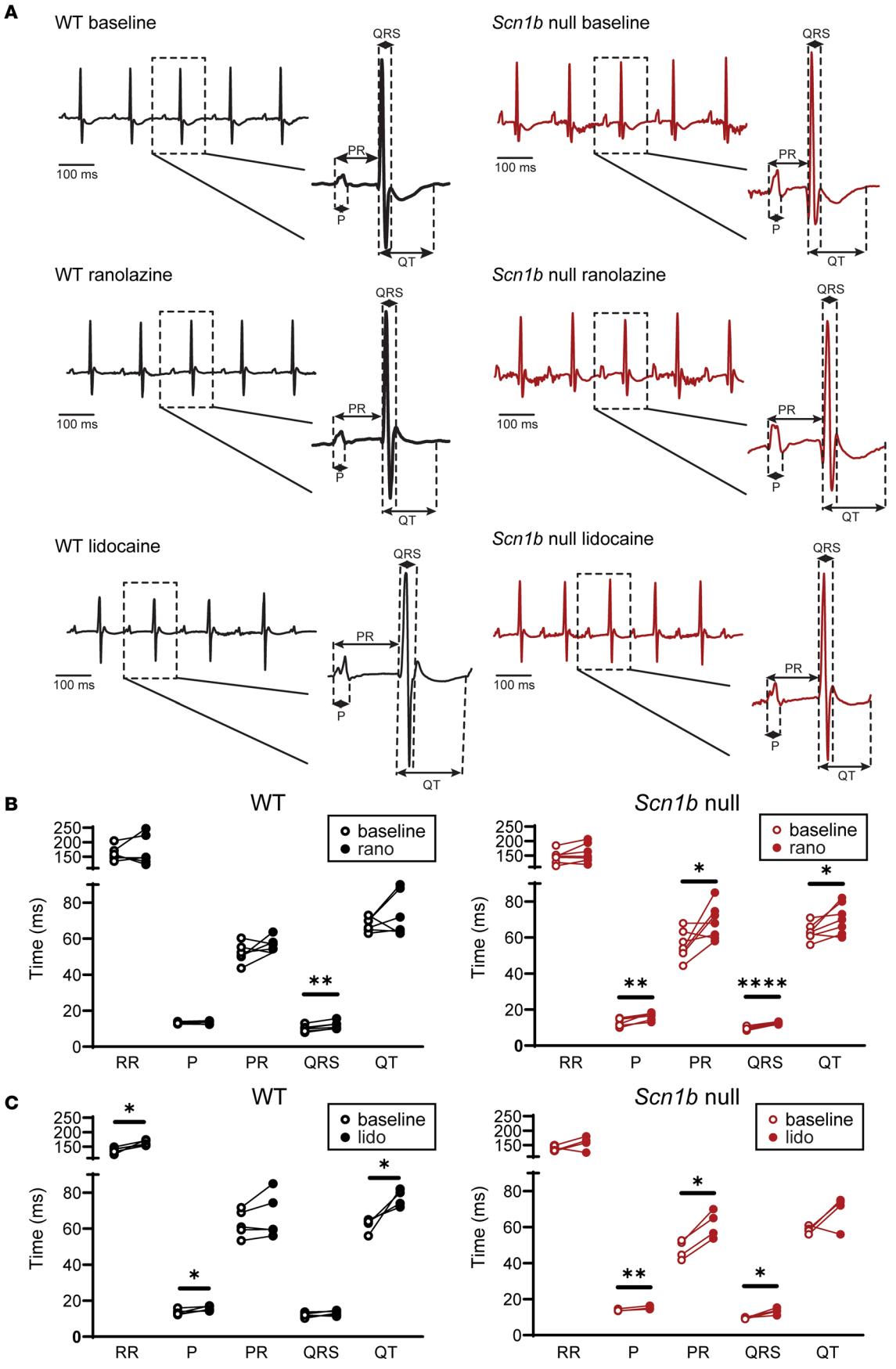
A
WT baseline
Scn1b null baseline
WT ranolazine
Scn1b null ranolazine
WT lidocaine
Scn1b null lidocaine
100 ms
QRS
PR
P
QT
B
WT
Scn1b null
baseline
rano
Time (ms)
RR
P
PR
QRS
QT
C
WT
Scn1b null
baseline
lido

Figure 6. ECG recordings from WT and *Scn1b*-null mice before and after ranolazine or lidocaine injections. (**A**) Representative ECG recordings obtained from WT and *Scn1b*-null mice at baseline, postranolazine, and postlidocaine are presented. The postranolazine and postlidocaine data were recorded 10 minutes after the i.p. injections of ranolazine or lidocaine. P wave durations, PR, QRS, and QT intervals were measured as indicated in the insets. (**B**) Comparison of ECG parameters measured in WT (left panel) and *Scn1b*-null (right panel) mice at baseline and 10 minutes after i.p. injections of ranolazine injection. Ranolazine markedly prolonged the P wave duration and the PR interval in *Scn1b*-null but not in WT mice. (**C**) Comparison of ECG parameters measured in WT (left panel) and Scn1b-null (right panel) mice at baseline and 10 minutes after i.p. injections of lidocaine. Lidocaine markedly prolonged the RR interval, P wave duration, and QT interval in WT mice. In *Scn1b*-null mice, lidocaine also prolonged the P wave duration and resulted in marked prolongation of the PR and QRS intervals. Each data set represents data from 4–7 mice. The ECG parameters and statistical comparisons are shown in Supplemental Table 1.

of the $Na_V\beta$ subunits. However, with the $Na_V\beta1$ subunit present, the lidocaine effect on the DIII-VSD was enhanced, whereas the ranolazine effect was blunted. Conversely, $Na_V\beta3$ enhanced ranolazine-induced DIII-VSD stabilization while inhibiting the effect of lidocaine. The differential regulation of the DIII-VSD resulted in distinct effects on the potencies of lidocaine and ranolazine depending on which $Na_V\beta$ was present. Thus, despite the similarity of the chemical structures (Figure 1), the therapeutic responses to lidocaine and ranolazine were differentially modified by the coexpression of the $Na_V\beta1$ or the $Na_V\beta3$ subunit.

$Na_V\beta1/\beta1B$ modulates class Ib antiarrhythmic responses from molecular to the whole-heart level. In *Xenopus* oocytes, with VCF and cut-open voltage clamp recordings, we demonstrated that $Na_V\beta1$ coexpression enhanced lidocaine's but inhibited ranolazine's effect on the DIII-VSD, which resulted in an increased lidocaine but decreased ranolazine block. In addition, we observed increased UDB and late I_{Na} block by lidocaine but opposite effects with ranolazine in WT compared with *Scn1b*-null mouse LV myocytes. This cellular difference further led to distinct phenotypes of the in vivo ECG recordings in response to lidocaine and ranolazine injections. For example, in response to ranolazine injection, the P wave duration and PR interval were prolonged in the *Scn1b*-null mice but not in the WT mice. This difference in ECG parameters reflects the cellular phenotype of enhanced ranolazine block of I_{Na} in *Scn1b*-null compared with WT LV myocytes. However, not all the ECG changes can be explained by the differences observed in myocyte I_{Na} recordings of atrial and ventricular myocytes, and they may be caused by $Na_V\beta1$-mediated effects on other regions of the myocardium, such as the sinoatrial and atrioventricular nodes (40). Alternatively, $Na_V\beta1$ may affect drug interactions with other ion channels that regulate cardiac excitation, as discussed further below.

Differential expression of $Na_V\beta1/\beta1B$ in human atria and ventricles and chamber-specific drug responses. Ranolazine was proposed as a candidate for atrial specific therapy for AF (24, 41). Studies in the canine heart showed that atrial and ventricular cardiomyocytes have distinct responses to ranolazine (24). In the atria, ranolazine prolongs the action potential duration measured at 90% repolarization (APD_{90}) and effective refractory period (24). In contrast, in the ventricle, ranolazine shortens the APD_{90}. Here, we demonstrated higher *SCN1Ba* ($Na_V\beta1$) and *SCN1Bb* ($Na_V\beta1B$) subunit mRNA expression levels in human atria compared with ventricles. While we showed that $Na_V\beta1$ coexpression attenuated ranolazine block of I_{Na} in both *Xenopus* oocytes and mouse LV myocytes, higher levels of $Na_V\beta1$ in human atria may result in similar attenuation of the effects of ranolazine, thus contributing to decreased ranolazine blockade compared with ventricles. Notably, ranolazine is also a blocker of *KCNH2*–encoded (HERG-encoded) repolarizing I_{Kr} channels (22). If ranolazine blockade of I_{Na} is reduced in atria, modulation of I_{Kr} may dominate, resulting in prolongation of APD specifically in atria. Thus, the heterogeneous expression of $Na_V\beta1$ may play a role in the chamber-specific ranolazine response.

$Na_V\beta$ subunit modulation of class Ib drug effects may underlie disease-specific drug responses. A search of NCBI's Gene Expression Omnibus (GEO) profile database (42) revealed that *SCN1B* is upregulated in ischemic cardiomyopathies in human heart [GEO GDS651 and GDS1362 (43)] and mouse heart failure models [GEO GDS411, GDS427 (44), and GDS3660 (45)] (Supplemental Figure 6). These data suggest that the expression of $Na_V\beta$ subunits can be altered in disease remodeling of the cardiac tissue. Since late I_{Na} was found to be increased in the failing heart, class Ib drugs have become potential therapeutic approaches in targeting heart failure–related arrhythmias (46). As we have demonstrated that $Na_V\beta$ can differentially modulate class Ib effects, upregulation of $Na_V\beta1$ in failing tissue may alter the patient response to Na_V channel–targeting antiarrhythmic therapies.

Differential effects of $Na_V\beta$ subunits on lidocaine and ranolazine interactions reflect distinct molecular drug-pore interactions. Previous work postulated that both lidocaine and ranolazine bind to common residues in the $Na_V1.5$ channel pore (20, 31). However, we observed that lidocaine modulated both the DIII- and DIV-VSDs of $Na_V1.5$, whereas ranolazine only affected the DIII-VSD when $Na_V1.5$ was expressed without

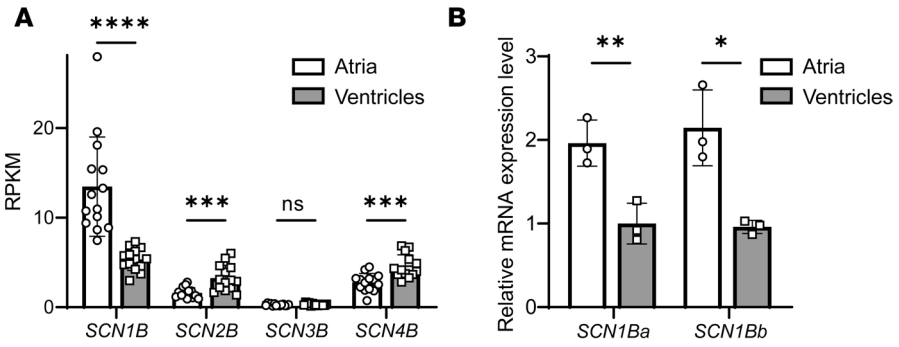

Figure 7. Regional differences in *SCN1B* expression in human atria and ventricles. (**A**) Extracted RNA-Seq data, expressed as reads per kilobase of exon per million mapped reads, from analyses of sequencing data obtained from matched (n = 8) human ventricular and atrial tissue samples (44). The *SCN1B* transcript was the most abundant of the $Na_V\beta$ subunits expressed in human atria and ventricles. In addition, *SCN1B* expression was approximately 3-fold higher in human atria compared with ventricles, whereas both *SCN2B* and *SCN4B* were approximately 2-fold higher in human ventricles than atria. (**B**) The differential expression of *SCN1B* in human atria and ventricles was confirmed by quantitative PCR (qPCR) analyses of the same paired human atrial and ventricular tissue samples analyzed by RNA-Seq. In addition, qPCR analyses using primers that distinguish the 2 *SCN1B* variants, *SCN1Ba* and *SCN1Bb*, revealed that the relative expression levels of both *SCN1Ba* and *SCN1Bb* transcripts were higher in the atria than the ventricles. Paired 2-tailed Student's t test was used to test significance. *$P < 0.05$; **$P < 0.01$; ***$P < 0.001$; ****$P < 0.0001$.

$Na_V\beta$ subunits, suggesting that these compounds may present in different orientations in the channel pore. Recent molecular dynamics simulations shed light on the detailed binding conformations of lidocaine and ranolazine within the $Na_V1.5$ channel (47). Interestingly, these studies revealed that 2 lidocaine molecules can bind to the pore concurrently, one to the F1760 site and the other to the central pore (47). In contrast, ranolazine binds to the F1760 residue and possesses a more flexible linear structure, allowing it to interact with a larger area ranging from the fenestration to the selectivity filter (47). Moreover, ranolazine has a pK_a of 7.2 (48) and lidocaine has a pK_a of 7.9 (49). At physiological pH, therefore, a higher percentage of ranolazine molecules are expected to be uncharged compared with lidocaine. This difference will determine the relative percentages of the drug molecules entering in the hydrophobic pathway through the fenestration versus the hydrophilic pathway via the intracellular gate. The presence of $Na_V\beta1$ or $Na_V\beta3$ modulates DIII-VSD and DIV-VSD dynamics, which can allosterically affect the conformation of the pore and fenestrations. We demonstrated that $Na_V\beta1/\beta3$'s modulation of ranolazine block was not entirely dependent on the main local anesthetic binding site, F1760, suggesting the changes in the DIII-VSD conformation due to $Na_V\beta$ modulation are essential for determining drug accessibility to the pore, independent of binding. In contrast, eliminating the F1760 binding site abolished the effects of $Na_V\beta1/\beta3$ coexpression on lidocaine block, further suggesting that lidocaine acts through mechanisms distinct from those of ranolazine. Because lidocaine and ranolazine have different stoichiometries, orientations within the pore, and entrance pathways, it is plausible that changing channel VSD and pore conformations in the presence of $Na_V\beta$ subunits can result in opposite effects on DIII-VSD interactions with these drugs.

$Na_V\beta$ subunit modulation of antiarrhythmic drug outcome beyond Na_V channels. Aside from Na_V channels, $Na_V\beta$ subunits have been shown to modulate expression and gating of various potassium channels, including the voltage-gated K_V 4.3 and the inward-rectifying K_{ir} 2.1 channels, resulting in modifications of 2 essential cardiac currents, the fast transient outward K^+ current ($I_{to,f}$) and the inward rectifier current (I_{K1}–) (50–52). Although unexplored to date, it also seems highly likely that the presence of $Na_V\beta$ subunits can affect K_V and K_{ir} channel pharmacology as well. Here, we showed that although single cardiac-specific *Scn1b*-null LV myocytes displayed attenuated inhibition of I_{Na} by lidocaine compared with WT cells, enhanced PR and QRS interval prolongation was observed in *Scn1b*-null animals with lidocaine, suggesting contributions from other cardiac ionic currents.

Limitations. To assess the drug effects on VSD dynamics, we conducted the VCF experiments in *Xenopus* oocytes. Because this is a heterologous expression system and the experiments were performed at 19°C, extrapolating the results to mammalian physiology can be difficult. However, we observed consistent drug-mediated modulatory effects in oocytes and in mouse LV myocytes, observations that support the hypothesis that the molecular mechanisms we identified with VCF are operative in mammalian systems.

We were only able to show that the expression of *SCN1B* was enriched in the atria compared with ventricles in the human heart at the transcript level. Although we attempted to examine protein expression levels directly, none of the available anti-$Na_V\beta1$ antibodies detect $Na_V\beta1$ proteins in mouse or human cardiac tissues. Since it is currently not possible to perform gene editing or to use siRNA-mediated knockdown strategies in native human myocytes, we were not able to explore the functional effects of $Na_V\beta1$ on class Ib drugs in human myocytes directly.

Conclusions. In summary, we have demonstrated roles for noncovalently linked $Na_V\beta$ subunits in regulating antiarrhythmic drug effects from molecular interactions to whole-heart phenotypes. Our results elucidated the differential regulation of $Na_V1.5$ channels by 2 class Ib agents, lidocaine and ranolazine, by $Na_V\beta1$ and $Na_V\beta3$ subunits. The unique expression profile of $Na_V\beta$ subunits in the human heart suggests chamber-dependent responses to these 2 compounds. Our findings provide crucial insights into strategies for improving the clinical outcomes of patients treated with class Ib agents for different forms of arrhythmias. Moreover, $Na_V\beta1$ expression is upregulated in heart failure, and it remains unexplored whether $Na_V\beta$ subunit expression is affected in other heart pathologies. This knowledge will be highly valuable in establishing disease-specific approaches to personalize arrhythmia treatment with lidocaine and ranolazine because known changes in β subunit expression will have predictable effects on therapeutic outcomes.

Methods

Experimental animals. Adult (8–15 weeks old) male and female WT and cardiac-specific *Scn1b*-null C57BL/6J mice were used in the experiments here. Cardiac-specific *Scn1b*-null mice were generated by crossing *Scn1b*^{fl} mice (27) with *B6.FVBTg*(*Myh6-cre*)*2182Mds/J* mice (The Jackson Laboratory), which express Cre recombinase driven by the α-myosin heavy chain promoter. Mice were genotyped by PCR analyses of genomic (tail) DNA using primers targeting sequences external to the *loxP* sites, as well as primers targeting Cre recombinase, as previously described (27). Because of the breeding strategy required to generate cardiac-specific *Scn1b*-null C57BL/6J mice, WT littermates were not generated. The WT mice used in the experiments presented here, therefore, were not littermate controls; rather they were WT C57BL/6J mice from our colony. Additional control experiments, however, were conducted on *Scn1b*^{fl} and *B6.FVBTg*(*Myh6-cre*)*2182Mds/J* mice, which were determined to be indistinguishable electrophysiologically from WT C57BL/6J animals. *Xenopus* oocyte harvests were performed as described previously (53).

Cut-open VCF. VCF experiments were conducted using 4 previously developed $Na_V1.5$ channel constructs (DI: V215C, DII: S805C, DIII: M1296C, DIV: S1618C) (53). Capped mRNAs were synthesized with the mMESSAGE mMACHINE T7 transcription kit (Life Technologies, Thermo Fisher Scientific) from the linearized pMAX vectors. VCF construct mRNA was injected alone or coinjected with *SCN1B* or *SCN3B* mRNA into *Xenopus* oocytes as previously described (14). VCF experiments were performed 4–6 days after injection. The recording setup and labeling protocol used were described previously (14, 53–55). Lidocaine hydrochloride and ranolazine dihydrochloride were dissolved in extracellular recording solution and then further diluted to 10 mmol/L and 4 mmol/L, respectively. Both drugs were manually perfused into the extracellular solution chamber in the cut-open voltage clamp setup. Fluorescence signals and currents were analyzed as previously described (18). $V_{1/2}$ values reported were quantified from the Boltzmann function fit, $y = 1/(1 + \exp [V - V_{1/2}]/k)$. Because the DIII F-V curve, especially under drug treatment conditions, did not saturate at the lowest voltage recorded (–160 mV), the fit was performed by fixing 0 at –200 mV. Because of the lack of saturation at the most negative potentials measured, the estimated $V_{1/2}$ for DIII F-V is likely to be higher than the actual $V_{1/2}$ value.

ECG recordings. Surface ECG recordings were obtained as previously described from mice anesthetized by i.p. injection of avertin (0.25 mg/kg; MilliporeSigma) (56). Baseline ECGs were recorded, and animals were weighed. For injections, drugs were dissolved in 250 μL PBS. Lidocaine or ranolazine was then injected at a dosage of 30 mg/kg or 20 mg/kg, respectively. Different animals were used for lidocaine or ranolazine injections. Between recordings, mice were kept on a heating pad maintained at 37°C ± 0.5°C. Postinjection ECGs were recorded at 5 minutes, 10 minutes, 15 minutes, 20 minutes, and 30 minutes. Peak responses were observed at 10 minutes, which was subsequently selected as the time point for ECG analysis.

RR, PR, and QT intervals, as well as P and QRS durations, were measured and compiled using Clampfit 10.3 (Molecular Devices) and GraphPad Prism. Note that QT intervals shown in figures were not corrected because several recent studies have shown that QT intervals in anesthetized mice do not vary with heart rate (57, 58). Similar differences were revealed, however, when corrected QT intervals were compared (Supplemental Table 1).

Isolation of adult mouse cardiomyocytes. Myocytes were isolated from adult (8 to 12 weeks old) WT or *Scn1b*-null mice as previously described (59). Briefly, hearts were isolated and perfused retrogradely through the aorta with a Ca^{2+}-free Earle's balanced salt solution containing 0.8 mg/mL type II collagenase (Worthington). After perfusion, the LV free wall was dissected and minced. The tissue pieces were then triturated to provide individual LV myocytes. Dispersed cells were then filtered and resuspended in Medium199 (Gibco, Thermo Fisher Scientific), plated on laminin-coated (MilliporeSigma) glass coverslips, and maintained in a 95% air/5% CO_2 incubator at 37°C.

Whole-cell Na_V current (I_{Na}) recordings were obtained from isolated LV myocytes at room temperature (22°C–24°C) within 5–6 hours of isolation using a Dagan 3900A amplifier interfaced to a Digidata 1332A A/D converter (Axon) using pClamp 10.2 (Axon). Recording pipettes contained the following (in mmol/L): 120 glutamic acid, 120 CsOH, 10 HEPES, 0.33 $MgCl_2$, 20 tetraethylammonium chloride (TEA-Cl), 4 Mg-ATP, 5 glucose, and 5 EGTA (pH adjusted to 7.3 with CsOH); pipette resistances were 1.5–3.0 MΩ. The bath solution contained the following (in mM): 20 mM NaCl, 110 mM TEACl, 4 KCl, 2 $MgCl_2$, 1 $CaCl_2$, 10 HEPES, and 10 glucose (pH 7.4; 300 mOsm).

Electrophysiological data were acquired at 10–20 KHz, and signals were low-pass-filtered at 5 kHz before digitization and storage. After the formation of a giga-seal (>1 GΩ) and establishment of the whole-cell configuration, brief (10 ms) ± 10 mV voltage steps from a holding potential (HP) of –70 mV were presented to allow measurements of whole-cell membrane capacitances (C_m), input resistances (R_{in}), and series resistances (R_s). In each cell, C_m and R_s were compensated electronically by approximately 85%; voltage errors resulting from uncompensated R_s were less than 2 mV and were not corrected. Leak currents were always less than 50 pA and were not corrected. Whole-cell I_{Na} were evoked in response to 40 ms voltage steps to potentials between –60 and +40 mV from an HP of –100 mV in 10 mV increments at 15-second intervals.

Electrophysiological data were compiled and analyzed using Clampfit 10.3 (Molecular Devices) and GraphPad Prism.

Quantitative reverse-transcription PCR. Total RNA (2 μg) isolated from individual matched (n = 6) human right atria, left atria, RV, and LV tissue samples was reverse-transcribed into cDNA with a high-capacity cDNA kit. Transcript analysis was conducted with SYBR green using a 7900HT Fast Real-Time PCR system (all from Applied Biosystems, Thermo Fisher Scientific). Data were analyzed using the Ct relative quantification method using the *GAPDH* and hypoxanthine guanine phosphoribosyl transferase I (*HPRT*) genes as endogenous controls.

Statistics. Results are presented as mean ± SEM. The number of animals and the number of cells used in each experiment are provided in the figure legends. Comparisons of differences between WT and *Scn1b*-null cells/animals under control conditions and before and after drug treatments were performed using a paired 2-tailed Student's t test (Microsoft Excel). In comparisons of more than 2 groups, 1-way ANOVA was used followed by multiple comparisons. The P values shown were corrected for multiple hypothesis testing using Dunnett's correction method. P values less than 0.05 were considered significant.

Study approval. All animals were handled in accordance with the NIH Guide for the Care and Use of Laboratory Animals, and all experimental protocols were approved by the Washington University IACUC.

Author contributions

WZ contributed to designing studies, conducting experiments, acquiring data, analyzing data, and writing the manuscript. WW, PA, and RLM contributed to conducting experiments and acquiring data. LLI contributed to providing experimental animals and editing the manuscript. JMN and JRS contributed to designing studies and editing the manuscript.

Acknowledgments

Human cardiac tissue samples were provided by the Translational Cardiovascular Biobank and Repository, supported by the Washington University Institute for Clinical and Translational Sciences, recipient of a Clinical and Translational Sciences Award (UL1 RR024992) from the NIH National Center for Research Resources.

Financial support was provided by the American Heart Association (predoctoral fellowship 15PRE25080073 to WZ); NIH National Heart, Lung, and Blood Institute (R01 HL136553 to JRS); NIH National Heart, Lung, and Blood Institute (R01 HL-034161 and R01 HL-142520 to JMN).

Address correspondence to: Jonathan Silva, Department of Biomedical Engineering, MSC 1097-202-190, Washington University in St. Louis, 1 Brookings Dr., Saint Louis, Missouri, 63130-4899 USA. Phone: 314.935.8837; Email: jonsilva@wustl.edu. Or to: Jeanne Nerbonne, Center for Cardiovascular Research, Department of Medicine, Cardiovascular Division, Washington University Medical School, 4939 Children's Place, Mail stop 8086-20-9900, St. Louis, Missouri 63110, USA. Phone: 314.362.2564; Email: jnerbonne@wustl.edu.

1. Zipes DP, Jalife J, eds. *Cardiac Electrophysiology: From Cell to Bedside: Sixth Edition*. Saunders; 2013.
2. Gellens ME, et al. Primary structure and functional expression of the human cardiac tetrodotoxin-insensitive voltage-dependent sodium channel. *Proc Natl Acad Sci U S A*. 1992;89(2):554–558.
3. Abriel H. Cardiac sodium channel Nav1.5 and interacting proteins: physiology and pathophysiology. *J Mol Cell Cardiol*. 2010;48(1):2–11.
4. Calhoun JD, Isom LL. The role of non-pore-forming β subunits in physiology and pathophysiology of voltage-gated sodium channels. *Hands Exp Pharmacol*. 2014;221:51–89.
5. Patino GA, et al. Voltage-gated Na+ channel 1B: a secreted cell adhesion molecule involved in human epilepsy. *J Neurosci*. 2011;31(41):14577–14591.
6. Rehm HL, et al. ClinGen — the clinical genome resource. *N Engl J Med*. 2015;372(23):2235–2242.
7. Gray B, et al. Lack of genotype-phenotype correlation in Brugada syndrome and sudden arrhythmic death syndrome families with reported pathogenic SCN1B variants. *Heart Rhythm*. 2018;15(7):1051–1057.
8. Yuan L, et al. Investigations of the Navβ1b sodium channel subunit in human ventricle; functional characterization of the H162P Brugada syndrome mutant. *Am J Physiol Heart Circ Physiol*. 2014;306(8):H1204–H1212.
9. Isom LL, et al. Primary structure and functional expression of the beta 1 subunit of the rat brain sodium channel. *Science*. 1992;256(5058):839–842.
10. Yan Z, et al. Structure of the Nav1.4-β1 complex from electric eel. *Cell*. 2017;170(3):470–482.
11. Pan X, et al. Structure of the human voltage-gated sodium channel Nav1.4 in complex with β1. *Science*. 2018;362(6412):eaau2486.
12. Shen H, et al. Structures of human Nav1.7 channel in complex with auxiliary subunits and animal toxins. *Science*. 2019;363(6433):1303–1308.
13. Jiang D, et al. Structure of the cardiac sodium channel. *Cell*. 2020;180(1):122–134.
14. Zhu W, et al. Mechanisms of noncovalent β subunit regulation of Na V channel gating. *J Gen Physiol*. 2017;149(8):813–831.
15. Salvage SC, et al. Gating control of the cardiac sodium channel Nav1.5 by its β3-subunit involves distinct roles for a transmembrane glutamic acid and the extracellular domain. *J Biol Chem*. 2019;294(51):19752–19763.
16. Muroi Y, Chanda B. Local anesthetics disrupt energetic coupling between the voltage-sensing segments of a sodium channel. *J Gen Physiol*. 2009;133(1):1–15.
17. Sheets MF, Hanck DA. Outward stabilization of the S4 segments in domains III and IV enhances lidocaine block of sodium channels. *J Physiol*. 2007;582(1):317–334.
18. Zhu W, et al. Predicting patient response to the antiarrhythmic mexiletine based on genetic variation: personalized medicine for long QT syndrome. *Circ Res*. 2019;124(4):539–552.
19. Moreno JD, et al. A molecularly detailed NaV1.5 model reveals a new class I antiarrhythmic target. *JACC Basic to Transl Sci*. 2019;4(6):736–751.
20. Ragsdale DS, et al. Common molecular determinants of local anesthetic, antiarrhythmic, and anticonvulsant block of voltage-gated Na+ channels. *Proc Natl Acad Sci U S A*. 1996;93(17):9270–9275.
21. Gianelly R, et al. Effect of lidocaine on ventricular arrhythmias in patients with coronary heart disease. *N Engl J Med*. 1967;277(23):1215–1219.
22. Antzelevitch C, et al. Electrophysiologic basis for the antiarrhythmic actions of ranolazine. *Heart Rhythm*. 2011;8(8):1281–1290.
23. Guerra F, et al. Ranolazine for rhythm control in atrial fibrillation: a systematic review and meta-analysis. *Int J Cardiol*. 2017;227:284–291.
24. Burashnikov A, et al. Atrium-selective sodium channel block as a strategy for suppression of atrial fibrillation: differences in sodium channel inactivation between atria and ventricles and the role of ranolazine. *Circulation*. 2007;116(13):1449–1457.
25. Antzelevitch C, et al. Electrophysiologic basis for the antiarrhythmic actions of ranolazine. *Hear Rhythm*. 2011;8(8):1281–1290.
26. Ramirez RJ, et al. Mechanisms by which ranolazine terminates paroxysmal but not persistent atrial fibrillation. *Circ Arrhythm Electrophysiol*. 2019;12(10):e005557.
27. Zareba W, et al. Ranolazine in high-risk patients with implanted cardioverter-defibrillators: the RAID trial. *J Am Coll Cardiol*. 2018;72(6):636–645.
28. Lin X, et al. Scn1b deletion leads to increased tetrodotoxin-sensitive sodium current, altered intracellular calcium homeostasis and arrhythmias in murine hearts. *J Physiol*. 2014;00(6):1–1407.
29. Arcisio-Miranda M, et al. Molecular mechanism of allosteric modification of voltage-dependent sodium channels by local anesthetics. *J Gen Physiol*. 2010;136(5):541–554.
30. Hanck DA, et al. Using lidocaine and benzocaine to link sodium channel molecular conformations to state-dependent antiarrhythmic drug affinity. *Circ Res*. 2009;105(5):492–499.
31. Ragsdale DS, et al. Molecular determinants of state-dependent block of Na+ channels by local anesthetics. *Science*. 1994;265(5179):1724–1728.
32. Hille B. Local anesthetics: hydrophilic and hydrophobic pathways for the drug-receptor reaction. *J Gen Physiol*. 1977;69(4):497–515.
33. Lopez-Santiago LF, et al. Sodium channel Scn1b null mice exhibit prolonged QT and RR intervals. *J Mol Cell Cardiol*.

2007;43(5):636–47.
34. Zhu W, et al. Conservation and divergence in NaChBac and NaV1.7 pharmacology reveals novel drug interaction mechanisms. *Sci Rep*. 2020;10(1):10730.
35. Johnson EK, et al. Regional differences in mRNA and lncRNA expression profiles in non-failing human atria and ventricles. *Sci Rep*. 2018;8(1):13919.
36. Zimetbaum P. Antiarrhythmic drug therapy for atrial fibrillation. *Circulation*. 2012;125(2):381–389.
37. Mazzanti A, et al. Gene-specific therapy with mexiletine reduces arrhythmic events in patients with long QT syndrome type 3. *J Am Coll Cardiol*. 2016;67(9):1053–1058.
38. Cha A, et al. Voltage sensors in domains III and IV, but not I and II, are immobilized by Na+ channel fast inactivation. *Neuron*. 1999;22(1):73–87.
39. Hsu EJ, et al. Regulation of Na^+ channel inactivation by the DIII and DIV voltage-sensing domains. *J Gen Physiol*. 2017;149(3):389–403.
40. Domínguez JN, et al. Temporal and spatial expression pattern of beta1 sodium channel subunit during heart development. *Cardiovasc Res*. 2005;65(4):842–850.
41. Zygmunt AC, et al. Mechanisms of atrial-selective block of Na+ channels by ranolazine: I. Experimental analysis of the use-dependent block. *AJP Hear Circ Physiol*. 2011;301(4):H1606–H1614.
42. Barrett T, et al. NCBI GEO: archive for functional genomics data sets — update. *Nucleic Acids Res*. 2013;41(Database issue):D991–D995.
43. Kittleson MM, et al. Gene expression analysis of ischemic and nonischemic cardiomyopathy: shared and distinct genes in the development of heart failure. *Physiol Genomics*. 2005;21(3):299–307.
44. Blaxall BC, et al. Differential myocardial gene expression in the development and rescue of murine heart failure. *Physiol Genomics*. 2003;15(2):105–114.
45. Wang T, et al. Particulate matter induces cardiac arrhythmias via dysregulation of carotid body sensitivity and cardiac sodium channels. *Am J Respir Cell Mol Biol*. 2012;46(4):524–531.
46. Horvath B, Bers DM. The late sodium current in heart failure: pathophysiology and clinical relevance. *ESC Heart Fail*. 2014;1(1):26–40.
47. Nguyen PT, et al. Structural basis for antiarrhythmic drug interactions with the human cardiac sodium channel. *Proc Natl Acad Sci U S A*. 2019;116(8):2945–2954.
48. Peters CH, et al. Effects of the antianginal drug, ranolazine, on the brain sodium channel NaV1.2 and its modulation by extracellular protons. *Br J Pharmacol*. 2013;169(3):704–716.
49. Liu H, et al. Common molecular determinants of flecainide and lidocaine block of heart Na+ channels: evidence from experiments with neutral and quaternary flecainide analogues. *J Gen Physiol*. 2003;121(3):199–214.
50. Deschênes I, et al. Post-transcriptional gene silencing of KChIP2 and Navβ1 in neonatal rat cardiac myocytes reveals a functional association between Na and Ito currents. *J Mol Cell Cardiol*. 2008;45(3):336–346.
51. Deschênes I, Tomaselli GF. Modulation of Kv4.3 current by accessory subunits. *FEBS Lett*. 2002;528(1–3):183–188.
52. Edokobi N, Isom LL. Voltage-gated sodium channel β1/β1B subunits regulate cardiac physiology and pathophysiology. *Front Physiol*. 2018;9:351.
53. Varga Z, et al. Direct measurement of cardiac Na+ channel conformations reveals molecular pathologies of inherited mutations. *Circ Arrhythm Electrophysiol*. 2015;8(5):1228–1239.
54. Rudokas MW, et al. The Xenopus oocyte cut-open vaseline gap voltage-clamp technique with fluorometry. *J Vis Exp*. 2014;(85):1–11.
55. Zhu W, et al. Molecular motions that shape the cardiac action potential: insights from voltage clamp fluorometry. *Prog Biophys Mol Biol*. 2016;120(1–3):3–17.
56. Marionneau C, et al. Distinct cellular and molecular mechanisms underlie functional remodeling of repolarizing K+ currents with left ventricular hypertrophy. *Circ Res*. 2008;102(111):1406–1415.
57. Speerschneider T, Thomsen MB. Physiology and analysis of the electrocardiographic T wave in mice. *Acta Physiol (Oxf)*. 2013;209(4):262–271.
58. Roussel J, et al. The Complex QT/RR relationship in mice. *Sci Rep*. 2016;6(1):25388.
59. Brunet S, et al. Heterogeneous expression of repolarizing, voltage-gated K+ currents in adult mouse ventricles. *J Physiol*. 2004;559(pt 1):103–120.